

Lightweight Design of Magnetic Integrated Transformer for High Voltage Power Supply in Electro-Aerodynamic Propulsion System

Zhenxing Zhao , Jijia Zhu , Yu-Xing Dai , Jun Wang , Senior Member, IEEE, Yachao Yang, Zishun Peng , Student Member, IEEE, Qianming Xu , Member, IEEE, Yong Ning, and Songming He

Abstract—Electro-aerodynamic unmanned aerial vehicles (EAD-UAVs) have strict requirements for lightweight. Due to the heavy weight of magnetic components and insulation materials, the power source of the EAD-UAV, an LCC high voltage power supply (HVPS)'s specific power cannot meet the minimum requirements. To improve the specific power of LCC HVPS, this article will optimize the magnetic core, insulation materials, and magnetic integrated transformer structure. First, the weight-frequency relation of the high-voltage transformer core is derived, and it is shown that there is an optimal frequency to minimize the weight of the high-voltage transformer core. Then, for insulation material optimization, the existing method points out that the input parallel output series (IPOS) array structure can reduce the amount of insulation material. This article uses the structure. But this article combined with the optimal frequency proposed the number of array transformers and insulation design method. Next, for each transformer in the array, an asymmetric magnetic integrated transformer structure is proposed. Which realizes the resonant inductance integration. At the same time, the magnetic shunt can be adjusted according to the needs of the winding. So, this structure can improve the utilization rate of the transformer window, and reduce the weight of the magnetic core. Finally, a 619 W-rated laboratory prototype is designed to convert 140 V input to 40 kV output. The designed IPOS transformer array weighs is 213.5 g, the total weight of the HVPS is 423.9 g, and the specific power is 1.46 kW/kg, working at the optimal frequency of 101.2 kHz.

Manuscript received 17 March 2023; revised 24 May 2023; accepted 2 June 2023. Date of publication 8 June 2023; date of current version 28 July 2023. This work was supported in part by the Hunan Provincial Department of Education Youth Project under Grant 21B0671, in part by the State Key Laboratory of Power System and Generation Equipment under Grant SKLD21KM05, in part by the Hunan Provincial Department of Education Scientific Research Project under Grant 22A0512, in part by the Hunan Province Key Areas Research and Development Plan Project under Grant 2021GK2019. Recommended for publication by Associate Editor H. H.-C. Iu. (Corresponding authors: Jijia Zhu; Yu-Xing Dai.)

Zhenxing Zhao, Jijia Zhu, Yachao Yang, Yong Ning, and Songming He are with the College of Electrical and Information Engineering, Hunan Institute of Technology, Xiangtan 411104, China (e-mail: 22006@hnie.edu.cn; peterzhuhn@163.com; 21170@hnie.edu.cn; 19527@hnie.edu.cn; songminghe0004@163.com).

Yu-Xing Dai, Jun Wang, Zishun Peng, and Qianming Xu are with the College of Electrical and Information Engineering, Hunan University, Changsha 410012, China (e-mail: daiyx@hnu.edu.cn; junwang@hnu.edu.cn; 1243127393@qq.com; xqm@hnu.edu.cn).

This article has supplementary material provided by the authors and color versions of one or more figures available at <https://doi.org/10.1109/TPEL.2023.3283978>.

Digital Object Identifier 10.1109/TPEL.2023.3283978

Index Terms—Electro-aerodynamic propulsion, lightweight design, magnetic integration, magnetic shunt.

I. INTRODUCTION

ELECTRO-AERODYNAMIC unmanned aerial vehicles (EAD-UAVs) use the “Ion wind” as propulsion, and this new propulsion system has received extensive attention from scholars [1], [2], [3], [4], [5]. For aircraft, lightweight is very important [1]. Therefore, the first goal of the LCC high-voltage power supply (HVPS) which generates the “Ion wind” is lightweight, the specific power is usually used to measure the lightweight design level of the power supply [3]. However, the specific power of the HVPS in the existing EAD-UAV is usually between 1.15 and 1.18 kW/kg [2], [4]. There is a certain gap with the theoretical value of 1.2 kw/kg.

LCC resonant converters are widely used in HVPS, due to the soft switching, and high voltage gain, and can use the parasitic parameters of the transformer to achieve magnetic integration [6], [7], [8], [9]. In the HVPS of the EAD propulsion system, the researchers have adopted this topology [1], [2], [4]. The transformers in LCC HVPS account for a large proportion of weight [9], and the transformer leakage inductance cannot meet the full integration of the resonant inductor, so it is necessary to add external inductors, which leads to difficulties in the lightweight design. The optimization of magnetic devices is very important.

Increasing the operating frequency can reduce the weight of magnetic devices [10], [11], which is one of the methods to achieve lightweight. The high-voltage power supply designed by Gilmore et al. [2] works at 500 kHz, which effectively reduces the weight of the resonant inductance and transformer, and improves the lightweight level of the whole machine. However, it is still necessary to add an external inductor which accounts for 16.8% of the weight of the HVPS.

Magnetic integration technology can realize the integration of resonant inductors and parallel capacitors [12], [13], [14], [15], [16], [17], [18], [19], [20], which is often used to improve the power density of the power supply and also contributes to lightweight design [2]. Zhang et al. [12], Li et al. [13], Ansari et al. [14], and Tian et al. [15] inserted a magnetic shunt between primary and secondary transformers to integrate all external inductors into the transformer, significantly improving

the power density of the whole machine. But this method is a low-voltage planar transformer integration scheme. In [16] and [17], a transformer magnetic core with multiple columns is designed, and multiple auxiliary windings are wound, respectively, on each intermediate column to realize the integration of external inductors and improve the power density of the whole machine. However, this scheme requires additional core columns, which is bad for lightweight. In [18], the parasitic capacitor of the transformer is used to integrate the parallel capacitor into the transformer. This method is only applicable to the high-power transformer with a low turn-to-turn coupling degree. If it is used to design the low-power transformer with a high coupling degree, the error will be larger. Dalessandro et al. [19] and Chagas and Marchesan [20] provided an accurate and universal calculation method for transformer parasitic capacitance, but in *LCC HVPS*, the parasitic capacitance of the rectifier should also be considered.

Most of the existing magnetic integration schemes aim at improving power density and are applied in low voltage. There is less research on the lightweight design of high-voltage power supply, and the lightweight design relies on engineering experience. The method of improving frequency to reduce the weight of the magnetic core [2], [4] has limitations in high-voltage applications. The strength of insulating materials will decrease with the increase in frequency [21]. Adding insulation materials to ensure reliability will increase the weight of the transformer. On the other hand, High voltage transformers have large turn ratios and many secondary turns. The symmetrical structure proposed in [16] and [17] (magnetic shunt fixed in the middle of the magnetic core), which is designed for low voltage cannot be used in the HVPS. In addition, the insulation material increases the winding spacing, and the magnetic core designed by the traditional AP method cannot accommodate the winding. If the magnetic core with a larger AP value is used, the weight of the magnetic core will increase.

The concept was partially presented in [23]. This article is an extension of the conference paper. This article is aimed at a lightweight design method of the magnetic integrated transformer to improve the specific power of *LCC HVPS*.

To achieve lightweight design of high-voltage power supply. The contributions of this article are as follows.

- 1) The weight-frequency relationship of the high-voltage transformer core is proposed. The traditional AP method does not consider the impact of insulation materials on the window area of transformers in high-voltage applications. This article introduces the relationship between filling coefficient and frequency based on the traditional AP method, and combines the weight AP function and AP frequency relationship to obtain the weight frequency relationship used in high-voltage transformers. This relationship indicates that there is a frequency point (Optimal frequency) in the transformer that minimizes the weight of the transformer.
- 2) The transformer adopts the input parallel output series (IPOS) array structure, which can reduce the number of insulation materials. This article combined with the optimal frequency (From contribution 1) proposed the

number of array transformers and insulation design methods, this has not been proposed in previous studies. In this method, the AP value, the transform power and the weight ratio of the actual transformer are taken as the limiting conditions. And the optimal selection of insulation materials is analyzed.

- 3) An asymmetric magnetic integration structure is proposed for the transformers in the array, which realizes the integration of resonant inductors. At the same time, the position of the magnetic shunt can be adjusted according to the winding, it can improve the utilization of the transformer window and further reduce the weight of the inductor and magnetic core. This article gives the calculation method of the leakage inductance and parasitic capacitance of the lightweight magnetic integrated transformer. The parasitic capacitance includes the parasitic capacitance of the transformer winding and the voltage doubling circuit, which is verified by simulation.

The rest of this article is organized as follows. Section II is the lightweight design scheme of the magnetic integrated transformer. In Section III, the calculation methods of leakage inductance and parasitic capacitance of lightweight magnetic integrated transformers are given. Section IV gives the design method of this article, and verifies the correctness of the method through simulation and comparison with the scheme of MIT in [2]. Section V is the experimental results. The magnetic integrated transformer array (213.5 g) designed by the method in this paper is applied to a 140 V input and 40 kV/619 W output *LCC HVPS*, with a specific power of 1.46 kW/kg. Finally, Section VI concludes this article.

II. LIGHTWEIGHT DESIGN SCHEME OF MAGNETIC INTEGRATED TRANSFORMER

In this section, the AP-frequency relation of the high voltage transformer is proposed, the AP-frequency relation is substituted into the weight-AP relation, and the weight-frequency relation of the high voltage transformer is derived. This relationship indicates that the weight of the high-voltage transformer is minimum when working at the optimal frequency($f_{\text{weight_min}}$). Then, the selection method of the number of transformers in the IPOS array is proposed, and the insulating material and the insulating mode are analyzed for the lightweight design requirements. Finally, an asymmetric magnetic integrated transformer structure is proposed, which realizes the full integration of resonant inductors and is suitable for high-voltage transformers.

For the high-voltage power supply designed in this article, the following points need to be explained.

- 1) The input of the HVPS is lithium batteries. The UAV works with 37 lithium batteries (4.35 V per battery) as input, its input voltage will experience above, equal to, and below the rated input successively. To ensure the constant thrust of 3N, the power supply needs to work under 600 W/40 kV full load. Therefore, the voltage feedback loop is adopted in this article. Through the feedback loop, the output voltage and power can be stabilized.

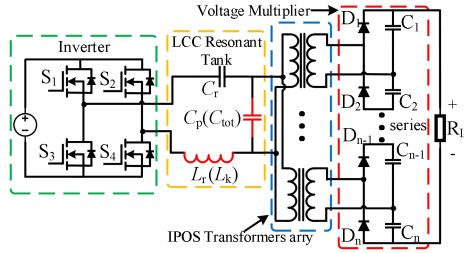


Fig. 1. Topology of the HVPS.

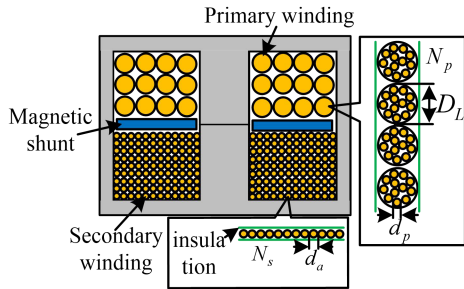


Fig. 2. Magnetic core and winding structure of transformer.

- 2) The high-voltage transformer has a large turn ratio and many secondary windings, so it is necessary to choose the magnetic core model with a larger window area under the same power. ER magnetic core has the maximum window area under the same processing power [28], and the transformer magnetic core in this article adopts ER series.

The topology of HVPS is shown in Fig. 1. The front stage is a full-bridge inverter. The resonant tank is composed of resonant capacitor C_r , parallel capacitor C_p , and resonant inductor L_r . The transformers use an IPOS array, each transformer is connected to the voltage multiplier, the voltage multiplier series output. In this scheme, transformer leakage inductance L_k is integrated with L_r , transformer and voltage multiplier parasitic capacitor C_{tot} is integrated with C_p , to realize the lightweight of the whole machine.

A. Optimal Frequency Selection for Lightweight Magnetic Integrated Transformer

The magnetic core and winding structure of the transformer is shown in Fig. 2. To simplify the analysis, assume the following.

- 1) The power supply works at the resonant frequency point, that is, $f = f_r = f_{\text{weight_min}}$.
- 2) The primary and secondary voltage waveforms of the transformer are duty cycle 0.5 square waves.
- 3) The primary and secondary current waveforms of the transformer are sine waves.

This design only discusses the case of two windings, the primary winding number is N_1 , the effective voltage value is V_1 , the effective current value is I_1 ; The number of secondary windings is N_2 , the effective voltage is V_2 , and the effective current is I_2 .

The derivation process of the weight-frequency relationship of the high-voltage transformer is as follows.

1) First, the AP-frequency relation of the high-voltage transformer is derived. According to Faraday's law, the column area A_{core} in the magnetic core is

$$A_{\text{core}} = \frac{0.5V_1}{2\pi N_1 f_{\text{eq}} B_m} \quad (1)$$

where B_m is the magnetic core flux density and f_{eq} is the equivalent switching frequency, V_1 is primary voltage. Since the transformer input is a square wave, f_{eq} is

$$f_{\text{eq}} = \frac{2}{\pi^2} f \frac{1}{D(1-D)} \quad (2)$$

where f is the actual switching frequency and D is the duty ratio.

In a high-voltage transformer, windings and insulating materials determine the size of the window area A_{window} , and the A_{window} of the high-voltage transformer is

$$A_{\text{window}} = \frac{N_1 I_1 + N_2 I_2}{K_u J_w} \quad (3)$$

where J_w is the current density; K_u is the window utilization factor. From experience, K_u as shown in Table XII, N_1 and N_2 are the primary and secondary windings, respectively.

Combined with (1) to (3), the AP value of high voltage transformer in the LCC converter is as follows:

$$AP = A_{\text{core}} A_{\text{window}} = \frac{\pi (I_1 N_1 + N_2 I_2) V_1}{32 N_1 f B_m J_w K_u}. \quad (4)$$

Since there are iron losses and copper losses in high-frequency transformers, which are related to B_m and J_w , respectively, B_m and J_w are both functions of frequency.

2) Derive the relationship between B_m , J_w , and frequency, respectively, and put it into (4) to obtain the relationship between AP and frequency.

First, the relationship between B_m and frequency is derived. The iron loss of the variable voltage magnetic core can be expressed as

$$\rho_{\text{loss_core}} = K_1(f) B_m^{K_2(f)} \quad (5)$$

where $\rho_{\text{loss_core}}$ is the loss density of the magnetic core, $K_1(f)$ and $K_2(f)$ are frequency-related coefficients, determined by the material of the magnetic core. The data can be seen in Table VIII. The relationship between flux and frequency can be deduced from (5)

$$B_m = \left[\frac{\rho_{\text{loss_core}}}{K_1(f)} \right]^{\frac{1}{K_2(f)}}. \quad (6)$$

Then, the relationship between J_w and frequency is derived. Proximity effect and skin effect in winding are ac loss, which can be expressed as

$$P_{\text{cop_loss}} = \rho_{\text{loss}} V_{\text{cop_tot}} = J_w^2 V_p F_p / \sigma + J_w^2 V_s F_s / \sigma \quad (7)$$

where $\rho_{\text{loss_cop}}$ is the copper loss density, $V_{\text{cop_tot}}$ is the total volume of the primary and secondary winding, V_p is the primary winding volume, F_p is the primary winding loss coefficient, V_s is the primary winding volume, F_s is the primary winding loss coefficient. In practical application, Litz wire is used to improve

the effective area, so ac loss model under thin wires is required. Ac loss coefficient F can be expressed as

$$\begin{aligned} F &= 1 + \frac{5N^2 n_i - 1}{45} (\pi \sigma f_{eq} K_i)^2 \left(\frac{I_{rms}}{J_w L_s} \right)^2 \\ &\approx 1 + \frac{N^2 n_i}{9} (\pi \sigma f_{eq} K_i)^2 \left(\frac{I_{rms}}{J_w L_s} \right)^2 \end{aligned} \quad (8)$$

where σ is the conductivity of copper and N is the number of primary or secondary winding layers; n_i is the number of shares and 1 for single winding; K_i is the filling coefficient between layers of the high voltage transformer, i represents the case of a single wire or Leeds wire. K_i for single wire and Litz wire is

$$K_{\text{alone}} = \frac{N_{\text{alone}} d_{\text{alone}}}{2l_{c1}} K_{\text{litz}} = \frac{\sqrt{\pi N_{\text{litz}}} d_{\text{litz}}}{2D_L} \quad (9)$$

where l_{c1} is the window length of the magnetic core; N_{alone} is the number of windings in each layer of the single wound wire; d_{alone} is the diameter of the single wound wire; N_{litz} is the number of windings in each layer of the Litz wire; d_{litz} is the diameter of the fine wound wire in the Litz wire; D_L is the total diameter of the Leeds wire; I_{rms} is the effective value of the current flowing through the winding.

Combined with (7) to (9), the current density can be obtained as (10) shown at the bottom of this page, where N_p and N_s are the primary and secondary layers, respectively. At this point, the relationship between J_w and frequency is obtained.

By substituting (6)–(10) into (4), AP - frequency is: (11) shown at the bottom of this page.

3) The weight-AP relation of the high-voltage transformer core is used as the intermediate relation to deducing the weight-frequency relation of the transformer core. The function of transformer core volume and winding volume as AP can be expressed as

$$\begin{aligned} V_{\text{core}} &= K_c A P^{0.75} \\ V_{\text{wind}} &= K_u K_w A P^{0.75} \end{aligned} \quad (12)$$

where K_c and K_w are constants. For ER core, they are 9.41 and 6.88, respectively. The transformer weight can be written as follows from the volume relation:

$$W_T = \rho_{cop} V_{\text{wind}} + \rho_{\text{core}} V_{\text{core}} = K_{wt} A P^{0.75} \quad (13)$$

$$J_w = \sqrt{\frac{\rho_{\text{loss_cop}} V_{\text{cop_tot}} \sigma - \frac{(\pi \sigma f_{eq})^2 [N_1 N_p K_{\text{litz}}^2 \left(\frac{I_1}{N_p} \right)^2 + N_2 N_s K_{\text{alone}}^2 \left(\frac{V_o I_2}{3M_i V_{in} N_s} \right)^2]}{9}}{2}} \quad (10)$$

$$AP = \frac{\pi (I_1 N_1 + N_2 I_2) V_1}{16 f K_u N_1 \left[\frac{\rho_{\text{loss_core}}}{K_1(f)} \right]^{\frac{1}{K_2(f)}} \sqrt{\left[\rho_{\text{loss_cop}} V_{\text{cop_tot}} \sigma - \frac{(0.81 \pi \sigma f)^2 [N_1 N_p K_{\text{litz}}^2 \left(\frac{I_1}{N_p} \right)^2 + N_2 N_s K_{\text{alone}}^2 \left(\frac{V_o I_2}{3M_i V_{in} N_s} \right)^2]}{9} \right]}} \quad (11)$$

where K_{wt} is 28.7 for ER core. By substituting (11) into (13), the weight-frequency relation of the transformer is (14) shown at the bottom of the next page.

The weight-frequency relationship of the high-voltage transformer can be obtained by Mathematica simulation, as shown in Fig. 3, and the data are shown in Table X. It can be seen from the figure that there is a frequency point $f_{\text{weight_min}}$, which minimizes the weight of the transformer. If the frequency is smaller than $f_{\text{weight_min}}$, increasing the working frequency can effectively reduce the weight of the magnetic core. When the value is greater than $f_{\text{weight_min}}$, the number of insulation materials increases and the spacing between windings increases. Therefore, the volume of the core is to be expanded to accommodate the windings and the weight of the transformer increases.

B. IPOS Transformer Array Design

This section conducts lightweight design based on the optimal frequency point $f_{\text{weight_min}}$. IPOS transformer array is used for lightweight design requirements. First, the selection method of the number of transformers in the IPOS array is proposed. Then, analysis of insulation materials and insulation methods; Finally, for the IPOS array of high-voltage transformers, an asymmetric magnetic integration structure is proposed, which realizes resonant inductance integration and makes full use of transformer window area.

a) *IPOS transformer array design*: The transformer with a single magnetic core has a large amount of insulation material, which is not conducive to the realization of a lightweight design. The solution uses an IPOS array to reduce the voltage stress of each transformer and reduce the use of insulation materials. To select the number of IPOS array transformers and realize the minimum array weight, the restriction conditions of transformers in the array need to be clear.

Restriction one is the minimum power of the transformer. To ensure basic power transmission, the minimum transmission power must be met. The minimum transmission power can be expressed as the minimum AP area

$$AP_{\min} \geq \frac{(1 + \eta) P_o}{4M\eta K'_u \beta J B f_r} \quad (15)$$

where f_r for resonance frequency is equal to the $f_{\text{weight_min}}$, η for the machine efficiency, J for current density, B is the core magnetic flux, and the whole bridge is 4.48 beta constant.

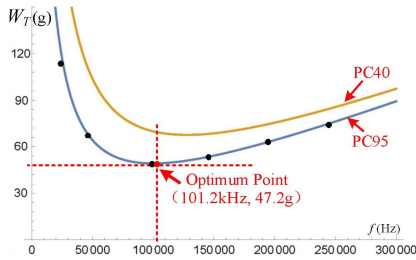


Fig. 3. Transformer weight frequency relation.

Considering the large amount of insulating material in the high-voltage transformer, the AP value should be considered as the average filling coefficient.

The second restriction condition is the designed redundancy to ensure that the transformer does not saturate. From the engineering experience, we can obtain

$$P_{\max} = \frac{1.2P_o}{\eta}. \quad (16)$$

The third restriction condition is the weight limit $\alpha W/W_t$ in lightweight design, where W is the total mass of the designed high-voltage power supply, α is the transformer weight ratio, and W_t is the weight of a single transformer.

M is the number of transformers in the IPOS transformer array, which consists of the above three constraints and is the smallest integer, which can be expressed as

$$\begin{cases} M_c = \left[\min\left(\frac{1.2P_o}{\eta P_t}, \frac{\alpha W}{W_t}\right) \right] \geq 2 \\ AP_{\min} \geq \frac{(1+\eta)P_o}{4M\eta K'_u \beta J B f} \end{cases} \quad (17)$$

where P_t is the power of a single transformer.

For high-voltage transformer, insulation reliability is related to the stability of the whole machine. To ensure the reliability of insulation and the lightest weight, the selection of insulation materials and treatment methods is one of the important links in the design. Table I lists the main insulating materials and insulating methods. It is necessary to carry out insulation test. The insulation test method is as follows: different materials are insulated in the corresponding way. Respectively, connected to the rectangular wave of 101.2 kHz, the rectangular wave voltage is gradually increased, and the transformer output voltage is measured until the transformer breakdown occurs. The voltage recorded at the time of breakdown is the transformer breakdown voltage.

TABLE I
INSULATION MATERIAL PARAMETERS AND INSULATION TESTING

Material	Density g/cm ³	strength kV/mm	Method	Transformer breakdown voltage(kV)
Teflon	2.2–2.5	0.6–1.5	coated	2.3
Epoxy resin	1.2–2.3	20–25	potting	4.7
Insulating oil	0.7–0.9	24–30	oil-immersed	5.1
Rubber	0.9–1.9	1–41	potting	4.4
Polyurethane	0.7–1.0	30–50	potting	10.2

Teflon bushings are insulated by wrapping secondary windings. Due to the large volume of bushings, the spacing between windings will increase, and expanding the magnetic core to accommodate the winding is not conducive to a lightweight design. Compared with Teflon tube-coated insulation, potting, and oil immersion have smaller spacing between windings and smaller core volume, which is more conducive to reducing the weight of the magnetic core.

The transformer oil is liquid at normal temperature. The high-voltage transformer designed in this scheme needs to be installed in the engine room of the UAV, and cannot be insulated by means of oil immersion. It is best to choose the insulating material that can solidify at normal temperature. Compared with rubber and polyurethane, the density of polyurethane is lower than that of rubber and the insulation strength is higher. In summary, for the lightweight high-voltage power supply designed in this article, polyurethane is used for potting insulation.

b) *Asymmetric magnetic integrated transformer*: IPOS array can reduce the amount of insulation in high-voltage transformers, but most of them are low-voltage transformers (Compared to the voltage in this article). Therefore, the symmetrical structure of the magnetic shunt located in the middle of the magnetic core (low voltage applications) cannot be used. This article presents an asymmetric magnetic integrated transformer structure suitable for high-voltage transformers.

The structure of the asymmetric magnetic integrated transformer is shown in Fig. 4. As shown in Fig. 4(a), the magnetic shunt ring is nested on the core column, and magnetic leakage is formed through the magnetic shunt to integrate the resonant inductor. The distance from the primary winding is x_p , and the distance from the secondary winding is x_s . As shown in Fig. 4(b), air gap 1 and 2 are located, respectively, between the edge

$$W_T = K_{wt} \left[\frac{\pi (I_1 N_1 + N_2 I_2) V_1}{16 f K_u N_1 \left[\frac{\rho_{loss_core}}{K_1(f)} \right]^{\frac{1}{K_2(f)}} \sqrt{\left[\rho_{loss_cop} V_{cop_tot} \sigma - \frac{(0.81\pi\sigma f)^2 \left[N_1 N_p K_{litz}^2 \left(\frac{I_1}{N_p} \right)^2 + N_2 N_s K_{alon}^2 \left(\frac{V_o I_2}{3M_i V_{in} N_s} \right)^2 \right]}{9} \right]}} \right]^{0.75}. \quad (14)$$

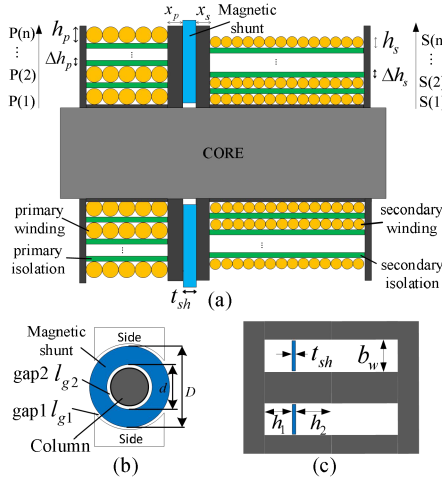


Fig. 4. Transformer structure with magnetic shunt (a) left view, (b) center view, and (c) top view.

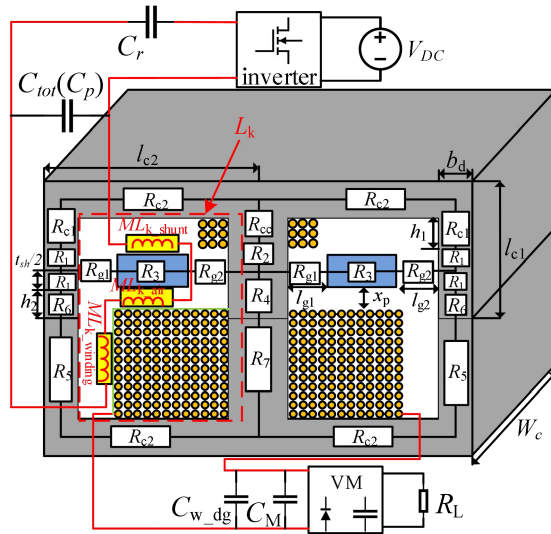


Fig. 5. Lightweight magnetic integrated transformer model.

column and the middle column of the magnetic core. As shown in Fig. 4(c), h_1 and h_2 can be freely adjusted according to the windings to fully utilize the window area and reduce the volume of the magnetic core, thus effectively realizing lightweight.

Where the weight of the magnetic diverter is

$$W_{\text{shunt}} = \pi t_{sh} \left[\left(\frac{D}{2} \right)^2 - \left(\frac{d}{2} \right)^2 \right] \rho_{\text{shunt}} \quad (18)$$

where t_{sh} is the thickness of the magnetic shunt, D is the outer diameter of the magnetic shunt, d is the inner diameter of the magnetic shunt, and ρ_{shunt} is the density of the magnetic shunt.

III. PROPOSED ASYMMETRIC INTEGRATED TRANSFORMER STRUCTURE

The asymmetric magnetic integrated transformer model is shown in Fig. 5. To achieve lightweight, resonant inductance L_r

is integrated with leakage inductance L_k , and parallel capacitor C_p is integrated with equivalent capacitance (C_{tot}). In this section, the leakage sensing L_k and the parasitic capacitance C_{tot} of the asymmetric magnetic integrated transformer will be introduced. The resonant inductor is mainly integrated through the magnetic shunt, so the thickness(t_{sh}) of the magnetic shunt is an important parameter. The equivalent parasitism (C_{tot}) of transformer and rectifier can be used to integrate some parallel capacitors, so the equivalent parasitism is also an important parameter.

A. Transformer Leakage Inductance

The leakage inductance L_k includes magnetic shunt leakage inductance (L_{k_shunt}), winding leakage inductance ($L_{k_winding}$), gap x_p , and x_s leakage inductance (L_{k_air}). The relationship among them is as follows:

$$L_k = M(L_{k_air} + L_{k_winding} + L_{k_shunt}). \quad (19)$$

When the transformer core and the number of turns are given, $L_{k_winding}$ and L_{k_air} can be obtained. The leakage induction only needs to be designed as L_{k_shunt} . The thickness t_{sh} determines the size of L_{k_shunt} [13], so the essence of magnetic shunt calculation is to get the t_{sh} value.

According to the energy relation of the inductor, $L_{k_winding}$, and L_{k_air} can be obtained as

$$E = \frac{1}{2} \int_V B \times H dV = \frac{1}{2} L_{k_i} I^2 \quad (20)$$

where E is inductive energy storage, V is the effective volume, B is the magnetic flux density, H is the field intensity, L_{k_i} is the leakage inductance of each part, and I is the current value.

a) *Leakage inductance in air and winding:* The energy stored in gaps x_p and x_s is [12]

$$L_{k_air} = 2\mu_0 \text{MTL}(N_p) \frac{(N_1 I_1)^2}{b_w} (x_p + x_s). \quad (21)$$

Leakage inductance formed by gaps of x_p and x_s is

$$L_{k_air} = 2\mu_0 \text{MLT}(N_p) \frac{(N_1)^2}{b_w} (x_p + x_s). \quad (22)$$

In the same way, the leakage inductance of primary and secondary winding is

$$\begin{aligned} L_p &= \frac{k_p^2 \mu_0 \text{MTL}(N_p)}{6b_w} [2h_p N_p^3 + \Delta h_p (2N_p^3 - 3N_p^2 + N_p)] \\ L_s &= \frac{k_s^2 \mu_0 \text{MLT}(N_s)}{6b_w} [2h_s N_s^3 + \Delta h_s (2N_s^3 - 3N_s^2 + N_s)] \\ L_{k_winding} &= L_p + L_s \end{aligned} \quad (23)$$

where $\text{MTL}(N_p)$ is the average length of the primary winding, $\text{MLT}(N_s)$ is the average winding length of the secondary winding, μ_0 is the relative permeability of air, h_p and h_s are the thickness of the primary winding and secondary windings, Δh_p and Δh_s are the insulation thickness of the primary winding and secondary windings, k_s is the number of secondary windings per layer, and k_p is the number of primary winding per layer.

b) Leakage inductance in magnetic shunt: The leakage inductance formed by magnetic shunt can be obtained by reluctance analysis. Therefore, first, the reluctance relation of the proposed magnetic integrated transformer is given. The reluctance of the magnetic integrated transformer is shown in Fig. 5. The parameters are given

$$R_m = R_{c2} + 0.5(R_{c1} + R_5 + R_6) + R_1 + R_4 + R_7 + R_2 + R_{cc}$$

$$\begin{aligned} R_{c1} &= \frac{h_1}{\mu_i b_d W_C} R_{c2} = \frac{l_{c2}}{\mu_i b_d W_C} R_{cc} = \frac{h_1}{\mu_i A_C} R_g = \frac{l_{g2}}{t_{sh} W_C} \\ R_1 &= \frac{t_{sh}}{2\mu_i b_d W_C} R_2 = \frac{t_{sh}}{2\mu_i A_C} R_3 = \frac{b_w - 2l_g}{\mu_i t_{sh} W_C} \\ R_4 &= \frac{0.5t_{sh} + h_2}{\mu_i A_C} R_5 = \frac{l_{c1}}{\mu_i b_d W_C} R_6 = \frac{h_2}{\mu_i b_d W_C} R_7 = \frac{l_{c1}}{\mu_i A_C} \end{aligned} \quad (24)$$

where A_c is the area of the transformer magnetic column, μ_i is the relative permeability of the magnetic core, μ_s is the relative permeability of magnetic shunt, l_{g1} is the width of air gap 1, l_{g2} is the width of air gap 2, l_{g2} and l_{g1} are equal, and the dimensions of l_{c1} , l_{c2} , b_d , and W_c are shown in Fig. 5.

Then, the leakage sensation formed by the magnetic shunt is pushed through the reluctance relation. The primary and secondary voltage of the transformer and reluctance is

$$\begin{bmatrix} V_p \\ V_s \end{bmatrix} = \begin{bmatrix} L_{PP} & L_{PS} \\ L_{SP} & L_{SS} \end{bmatrix} \frac{d}{dt} \begin{bmatrix} i_p \\ i_s \end{bmatrix} = \begin{bmatrix} L_{k_shunt} + L_m & \frac{N_s}{N_p} L_m \\ \frac{N_s}{N_p} L_m & L_{k_shunt} + (\frac{N_s}{N_p})^2 L_m \end{bmatrix} \frac{d}{dt} \begin{bmatrix} i_p \\ i_s \end{bmatrix} \quad (25)$$

where L_{pp} and L_{ss} are the self-inductance of the primary and secondary winding of the transformer, L_{ps} , and L_{sp} are the mutual inductance of the transformer, and L_m is the inductance of the transformer excitation.

Leakage inductance produced by magnetic shunt is

$$L_{k_shunt} = 2(L_{PP} - L_m). \quad (26)$$

According to (25), and (26) and the magnetic relationship, the excitation inductance, and primary self-induction can be expressed as

$$\begin{aligned} L_m &= \frac{N_p}{N_s} L_{PS} = \frac{N_p N_s}{N_s I_1} = \frac{N_p}{I_1} \phi_{ps} \\ L_{PP} &= \frac{N_p^2}{R} \end{aligned} \quad (27)$$

where ϕ_{ps} is the flux generated by the primary winding and flowing into the secondary, and R is the primary equivalent reluctance, which is given by

$$\begin{aligned} \phi_{ps} &= \frac{2N_1 I_1 (R_3 + 2R_g)}{R_m [R_m + 2(R_3 + 2R_g)]} \\ R &= \frac{R_m [R_m + 2(R_3 + 2R_g)]}{R_m + [R_m + 2(R_3 + 2R_g)]}. \end{aligned} \quad (28)$$

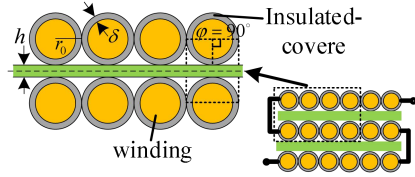


Fig. 6. Transformer secondary winding structure.

From (26) to (28), leakage inductance L_{k_shunt} can be expressed as

$$L_{k_shunt} = \frac{4N_1^2}{R_m + 2(R_3 + 2R_g)}. \quad (29)$$

From (29), the thickness of the magnetic shunt is

$$t_{sh} = \frac{c_1 + \sqrt{c_2 + c_3}}{A_C + 2b_d W_c} \quad (30)$$

where parameters c_1 , c_2 , c_3 , a , and b can be expressed as

$$c_1 = b A_C b_d u_0 u_i W_c - b_d h_2 W_c - a A_C b_d u_0 u_i W_c$$

$$c_2 = 8(A_C b_d l_g - 0.5 A_C b_d b_w - A_C b_d l_g u_i)(A_C + 2b_d W_c)$$

$$c_3 = (b A_C b_d u_0 u_i W_c - b_d h_2 W_c - a A_C b_d u_0 u_i W_c)^2$$

$$a = R_{c2} + 0.5(R_{c1} + R_5 + R_6) + R_7 + R_{cc}$$

$$b = 4k_p^2 N_p^2 / LL = (L_r - M L_{k_winding} - M L_{k_air}) / M. \quad (31)$$

The magnetic integration method of high voltage transformer with magnetic shunt is analyzed in this section. Equations (22) and (23) are the values of L_{k_air} and $L_{k_winding}$. Equation (29) is the values of L_{k_shunt} . Equations (30) and (31) are the calculation method of magnetic shunt thickness. Using these three leakage inductors, the L_r is integrated into the transformer, which saves the external inductance and, thus, achieves lightweight.

B. Transformer Parasitic Capacitance

Due to the large turn ratio of the high-voltage transformer, the parasitic capacitances (C_{w_dg} and C_{eq_M}) of the transformer secondary and the voltage multipliers will form a large equivalent capacitance (C_{tot}) in the primary of the transformer. Using C_{tot} can realize parallel capacitor integration [19], [20], which improves the lightweight level of the whole machine. Although the equivalent parasitic capacitor can only be used passively to integrate part of the parallel capacitor, some weight can be reduced in here.

a) Parasitic capacitance in winding: The secondary winding structure of the transformer is shown in Fig. 6. Assuming that the windings of each layer are parallel ($\varphi = 90^\circ$), the secondary current and voltage of the transformer do not alternate. The static capacitance between layers can be obtained as

$$C_0 = \frac{N_{L-L} \varepsilon_0 \text{MILT}(N_S)}{1 - \delta/\varepsilon_D r_0} \left[V + \frac{1}{8\varepsilon_D} \left(\frac{2\delta}{r_0} \right) \frac{Z}{1 - \delta/\varepsilon_D r_0} \right]. \quad (32)$$

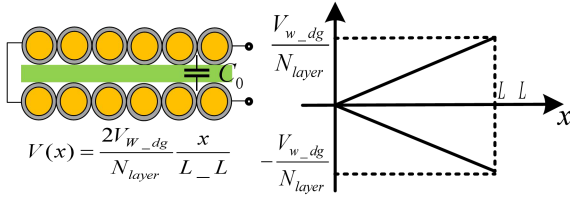


Fig. 7. Relationship between the potential of the “U” winding method and the horizontal distance.

The parameters in (32) are

$$\begin{aligned} V &= \frac{\beta}{\sqrt{\beta^2-1}} \arctan\left(\sqrt{\frac{\beta+1}{\beta-1}}\right) - \frac{\pi}{4} \\ Z &= \frac{\beta(\beta^2-2)}{3\sqrt{(\beta^2-1)^2}} \arctan\left(\sqrt{\frac{\beta+1}{\beta-1}}\right) - \frac{\pi}{4} - \frac{\beta}{2(\beta^2-1)} \\ \alpha &= 1 - \frac{\delta}{\varepsilon_D r_0} \beta = \frac{1}{\alpha} \left(1 + \frac{h}{2\varepsilon_F r_0}\right) \end{aligned} \quad (33)$$

where δ is the thickness of the winding insulation, r_0 is the radius of the winding, h is the thickness of the insulating medium between the two layers, ε_D is the dielectric constant of the winding insulation, ε_F is the dielectric constant of the insulating medium between the two layers, and N_{L-L} is the turn of each layer number.

However, the actual transformer voltage and current are alternated, and the equivalent capacitance in the ac state is required. As shown in Fig. 7, which is the relationship between the potential of the “U” winding method and the horizontal distance, the energy storage is

$$E_{L-L} = \frac{C_0}{2L} \int_0^{L-L} V^2(x) dx = \frac{2C_0}{3} \left(\frac{V_{w_dg}}{N_{layer}} \right)^2 \quad (34)$$

where C_{layer} is the equivalent capacitance between layers, V_{w_dg} is the voltage between layers, and $V(x)$ is a function of voltage and distance x .

From the energy storage-voltage relationship of the capacitor C_{layer} is

$$C_{layer} = \frac{C_0}{3} \quad (35)$$

where N_{layer} is the number of layers of the winding, K is the turns ratio of the transformer, and C_{w_eq} is the equivalent capacitance from C_{w_dg} to the primary.

If C_0 and C_{layer} in the winding do not change, the parasitic capacitance and equivalent capacitance in the whole winding are

$$\begin{aligned} C_{w_dg} &= \sum_{v=1}^{k_s-1} C_{Layer,v} \left(\frac{2}{N_s} \right)^2 = 4 \frac{k_s-1}{k_s^2} C_{layer} \\ C_{w_eq} &= MK^2 C_{w_dg} \end{aligned} \quad (36)$$

where k_s is the number of secondary windings per layer.

b) *Parasitic capacitance in voltage multipliers:* When the parallel capacitor is not clamped, the equivalent voltage multipliers are shown in Fig. 8. The filter capacitance is much larger than the high-voltage diode body capacitance. When the parallel capacitor is not clamped by the voltage, the capacitive reactance is dominated by the high-voltage diode body capacitance, and the conduction angle is θ . The FHA coefficients in the LCC

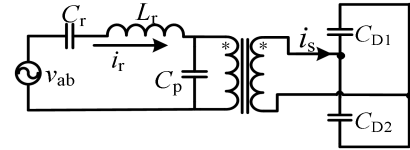


Fig. 8. Equivalent voltage multipliers when the parallel capacitor is not clamped.

converter are [23]

$$\begin{aligned} a_{v1} &= \frac{2}{\pi} \left[\frac{\sin \theta - \pi + \theta}{1 + \cos \theta} - \sin \theta \right] b_{v1} = \frac{2}{\pi} (1 - \cos \theta) \\ k_c &= \frac{2 \left[\frac{a_{v1}}{\sqrt{a_{v1}^2 + b_{v1}^2}} - \frac{1}{\pi} \sqrt{\frac{1}{4}(1 - \cos 2\theta)^2 + (\pi - \theta + \frac{\sin 2\theta}{2})^2} \right]}{\sqrt{a_{v1}^2 + b_{v1}^2} (1 + \cos \theta)} \end{aligned} \quad (37)$$

where a_{v1} and b_{v1} are the sine and cosine coefficients of the fundamental wave of the parallel capacitor voltage, and k_c is the coefficient between the parallel capacitor and the equivalent capacitance of the voltage multipliers.

Therefore, the equivalent capacitance of the voltage multipliers is

$$C_{eq_VM} = \frac{C_p k_c}{M}. \quad (38)$$

The C_p in (38) is

$$C_p = \frac{P^2 M N k_{VM} K^2}{2 f_s R_o \tan^2(\frac{\theta}{2})} \quad (39)$$

where k_{VM} is the voltage gain of the voltage multiplier, P is the number of voltage stages, M is the number of transformers, K is the turns ratio of the transformer, N is the number of stages of the voltage doubler rectifier, f_s is the switching frequency, R_o is the output load, and V_o is the output voltage.

C_{tot} is the equivalent parasitic capacitance formed by C_{w_dg} and C_{M_eq} , which is used for parallel capacitance integration. From (36) and (38), the C_{tot} is

$$C_{tot} = \frac{C_p k_c}{M} + MK^2 C_{w_dg}. \quad (40)$$

This section analyzes the parasitic capacitance of the high-voltage transformer. Equations (36) and (38) are the values of C_{w_dg} and C_M . By using these two parasitic capacitors, partial integration of C_p can be realized and the weight of the capacitor can be reduced.

IV. LIGHTWEIGHT DESIGN SCHEME AND VERIFICATION OF MAGNETIC INTEGRATED TRANSFORMER

This section reviews the design method of a lightweight magnetic integrated transformer and verifies the correctness of the magnetic integrated transformer model. First, a flow chart will be used to help sort out the relationship between parameters and make the design process clear. Then, the correctness of the proposed magnetic integrated transformer model is verified by finite element simulation combined with actual calculation. Finally, the parameters of the proposed scheme and the MIT scheme are compared. By comparing the two schemes, the

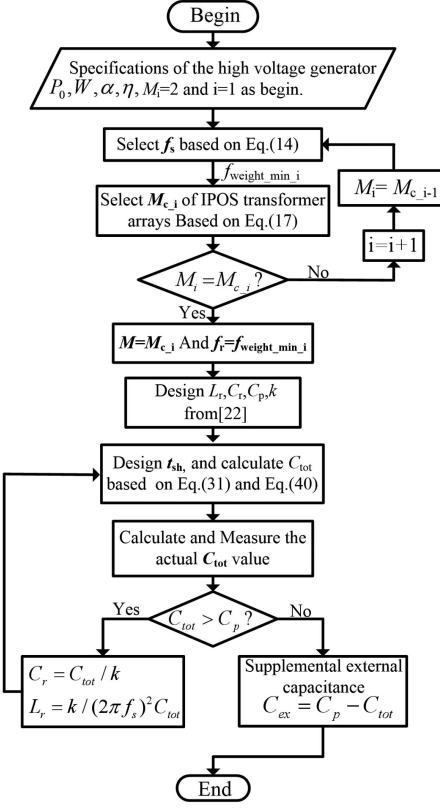


Fig. 9. Design flow chart of lightweight magnetic integrated transformer.

proposed scheme is reduced by 16.22%, which verifies the correctness of the proposed scheme.

A. Design Process of Lightweight Magnetic Integrated Transformer

The design process of a lightweight magnetic integrated transformer is shown in Fig. 9. The lightweight design process can be divided into two steps. First, select the optimal frequency $f_{\text{weight_min}}$ and the number of transformer arrays M according to the basic parameters of the high-voltage transformer. To enable the design algorithm to start, first, $M_1 = 2$ is substituted into (14) to select the optimal frequency $f_{\text{weight_min-1}}$, and this value is substituted into (17) to obtain M_{c-1} . Then, it is determined whether M_{c-1} and M_1 are equal. If not, M_{c-1} is returned to (14). Repeat the preceding steps i times until M_{c-i} equals M_i and proceed to the next step. In the second step, after determining the working frequency, the number of transformers M and the model, design the resonator parameters of the LCC converter (the selection of LCC resonator parameters can be referred to [22], which will not be repeated here), and select the appropriate insulation materials and insulation methods. The magnetic shunt t_{sh} is designed according to the resonant inductance required, and the parasitic capacitance C_{tot} of the transformer is calculated and measured to determine whether the external capacitor C_{ex} needs to be added or the magnetic shunt is redesigned according to C_{tot} .

TABLE II
MAGNETIC INTEGRATED TRANSFORMER PARAMETERS

t_{sh}	1.08 mm	l_{c1}	14.7 mm	l_g	0.1 mm
μ_i, μ_s	2300	l_{c2}	12.2 mm	b_d	4.2 mm
h_2	5.45 mm	W_c	11.5 mm	N_{pk_p}	15
h_1	6 mm	A_c	78.5 mm ²	I_p	1.07A

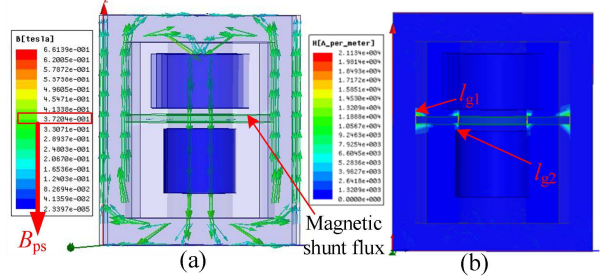


Fig. 10. Simulation of integrated transformer flux density. (a) Magnetic flux density simulation. (b) Magnetic field intensity simulation.

TABLE III
MAGNETIC INTEGRATION SCHEME AND APPLIED INDUCTANCE SCHEME PARAMETERS

integration	t_{sh}	d	D	ρ_{shunt}	W_{shunt}	W_{is_in}
Extra	1.08 mm	9.8 mm	22 mm	4.8g/cm³	$1.6 \times 4 = 6.4$ g	18.9 g
	core	I_{max}	ΔB_{max}		A_e	
	ER28 34	6A	0.25T		$81.4 \times 10^{-6} m^2$	
	AP	N	W_{core}	W_{cop}	W_L	W_{is_ex}
	1.21 cm ⁴	30	29.3 g	11.9 g	41.2 g	54.3 g

B. Verification of Lightweight Magnetic Integrated Transformer Model

According to the method in [22], the resonant cavity parameters were designed, and the required resonant inductance equal to the leakage inductance was 100.23 μ H. The parameters of the integrated transformer using the magnetic shunt are shown in Tables II and XI, and FEA simulation is performed after substituting the parameters, as shown in Fig. 10.

In Fig. 10, the visible magnetic flux passes through the magnetic shunt to form L_{k_shunt} . According to (21) to (25), B_{ps} can be calculated to be 0.396T, the simulation result is 0.372T, and the relative error is 6.45%.

By selecting the number of transformers according to (17), the required number of transformers M can be calculated as 4. The parameters of ER series magnetic core and related calculation results can be seen in Table IX. The same magnetic shunt is added to each transformer, the number of turns of primary and secondary windings is the same, and polytriamine vacuum potting insulation is adopted. The parameters of the lightweight integration scheme and the traditionally applied inductance scheme are shown in Table III (the material of the magnetic device is the same). The designed leakage inductance is 100.23 μ H, where

TABLE IV
PARAMETER COMPARISON BETWEEN THE SCHEME IN THIS ARTICLE
AND MIT [2]

Scheme Parameters \ Electrical Parameter	Parameters of MIT [2]	Parameters of this paper
Output voltage(kV)	40	40.1
Max Power(W)	750	800
Full-load efficiency (%)	85	87.3
Max efficiency (%)	85	90.1
Weight & Volume Parameter		
Heat sink weight(g)	89.2	43.6
Rectifier weight(g)	110.8	87.2
Inverter weight(g)	56	79.6 (Includes the drive and control circuit)
Magnetic device weight(g)	250	213.5
Total weight(g)	506	423.9
Magnetic device volume(mm^3)	57334	49560

$W_{\text{is_in}}$ is the insulation weight of the integrated scheme, and $W_{\text{is_ex}}$ is the insulation weight of the applied inductance scheme.

The weight of the magnetic shunt is calculated using the method in Section II-B. For the applied inductance scheme, the weight of the inductance winding is

$$W_{\text{cop}} = N \cdot l_{\text{av}} \cdot \frac{I_{\text{max}}}{J_{\text{cop_max(ac)}}} \cdot \rho_{\text{cop}}. \quad (41)$$

Furthermore, N is the turns of the inductance winding

$$N = \frac{LI_{\text{max}}}{\Delta B_{\text{max}} A_e} \quad (42)$$

where l_{av} is the average length of winding, I_{max} is the maximum effective value of the input current, $J_{\text{cop_max(ac)}}$ is the maximum current density of the copper wire under ac, ρ_{cop} is the density of copper, L is the required inductance, ΔB_{max} is the maximum flux swing, and A_e is the effective area of the core. The weight of the magnetic core can calculate the required AP value, select the magnetic core according to this value and obtain the weight parameter [10]. The inductor weight (W_L) is the sum of the core weight (W_{core}) and the copper wire weight (W_{cop}).

Through theoretical analysis and calculation, the integrated scheme is estimated to reduce 70.2 g by using a magnetic shunt and insulating materials. To verify the correctness of this method, an experimental platform designed by the proposed method was built, and MIT's scheme in [2] was compared. The parameters comparison between the two schemes was shown in Table IV. Due to the magnetic integration scheme of the magnetic shunt, the magnetic components in this scheme are reduced by 36.5 g, and the total weight is reduced by 82.1 g compared with the scheme of MIT.

TABLE V
MAIN PARAMETERS OF HVPS

K	M	P	N	k_M	f_s
25	4	1	1	2	101.2 kHz
V_{in}	V_o	P_o	η	W_{tot}	Trust
140V	40kV	600W	$\geq 85\%$	$\leq 440\text{g}$	3N

TABLE VI
LCC RESONANT TANK DESIGN PARAMETERS

Parameter	Value
Conduction angle θ	$\pi/3$
Parallel capacitor C_p	45.24 nF (30 nF+15 nF)
Resonant Inductance L_r	99.11uH
Resonant capacitor C_r	57.3 nF
Resonant frequency f_r	100 kHz

TABLE VII
MAGNETIC INTEGRATED TRANSFORMER PARAMETERS

Parameter	Value or Model
Leakage inductance L_k	99.13 uH
Equivalent parasitic capacitance C_{tot}	15.36 nF
Transformer Core	ER2834
The magnetic shunt device material	PC95
Thickness of the magnetic shunt	1.08 mm

V EXPERIMENTAL RESULTS

A. Experimental Platform Parameters

A 40 kV/600 W HVPS uses the magnetic integrated transformer designed by the proposed method. To ensure the specific power reaches 1.2 kW/kg, the total weight should not be over 500 g. The main parameters of the experimental platform are shown in Table V.

Based on the method in [22], LCC resonator parameters required by the high voltage converter can be calculated, as shown in Tables VI and VII. If no parasitic capacitor is used, the parallel capacitor (45.24 nF) must be 30 nF and 15 nF in parallel. Because C_{tot} realizes the integration of partial parallel capacitors, only one external parallel 30 nF capacitor is needed as a supplement, which can save a 15 nF capacitance and reduced by 1.3 g.

Fig. 11 shows the lightweight magnetic integrated transformer and the whole machine. The measured results show that the total weight is reduced by 71.2 g by using insulation material and a magnetic diverter, which is consistent with the analysis results in Section IV-B. Because of the use of the IPOS transformer array scheme, the transformer is reduced by an additional 26.4 g, indicating that the IPOS array can effectively improve the window utilization rate and reduce the core weight. Fig. 12 shows the experimental platform. The total weight of

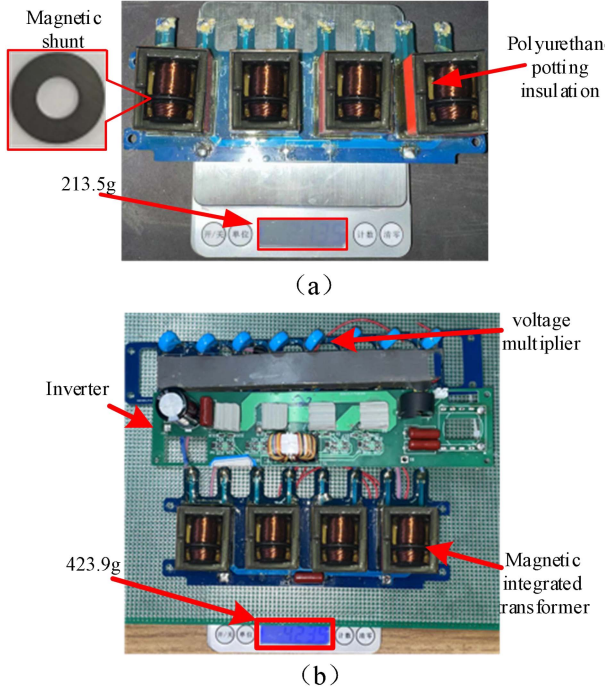


Fig. 11. High voltage power supply in this scheme. (a) Weight of the transformer in this article's scheme (including windings, magnetic cores, PCB, magnetic diverters, and insulation materials). (b) Weight of the whole machine in this article's scheme.

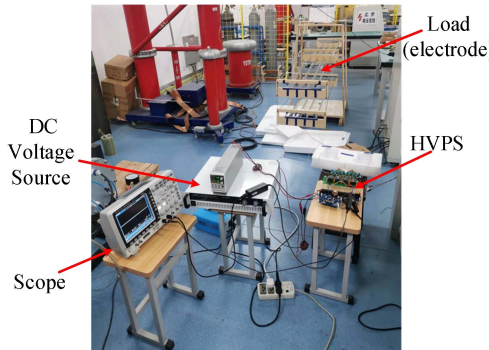


Fig. 12. Survey of experimental platform.

the high-voltage converter is 423.9 g, which is better than the expected design value of 440 g. The high voltage power supply adopts 37 polymer lithium batteries with high activity and high discharge rate (30 C). The input voltage is 140 V and the weight is 296.3 g.

B. Experimental Test Results

The waveforms of the HVPS at 140 V input, 40.1 kV output, and 619 W full load are shown in Fig. 13(a). Because the UAV needs a stable output of 40 kV to ensure the stability of thrust. To this end, a voltage feedback loop is designed in this article. When the battery voltage is higher than the rated input voltage, the frequency will be increased to maintain the output voltage and power. When the battery input voltage is 147 V, the feedback

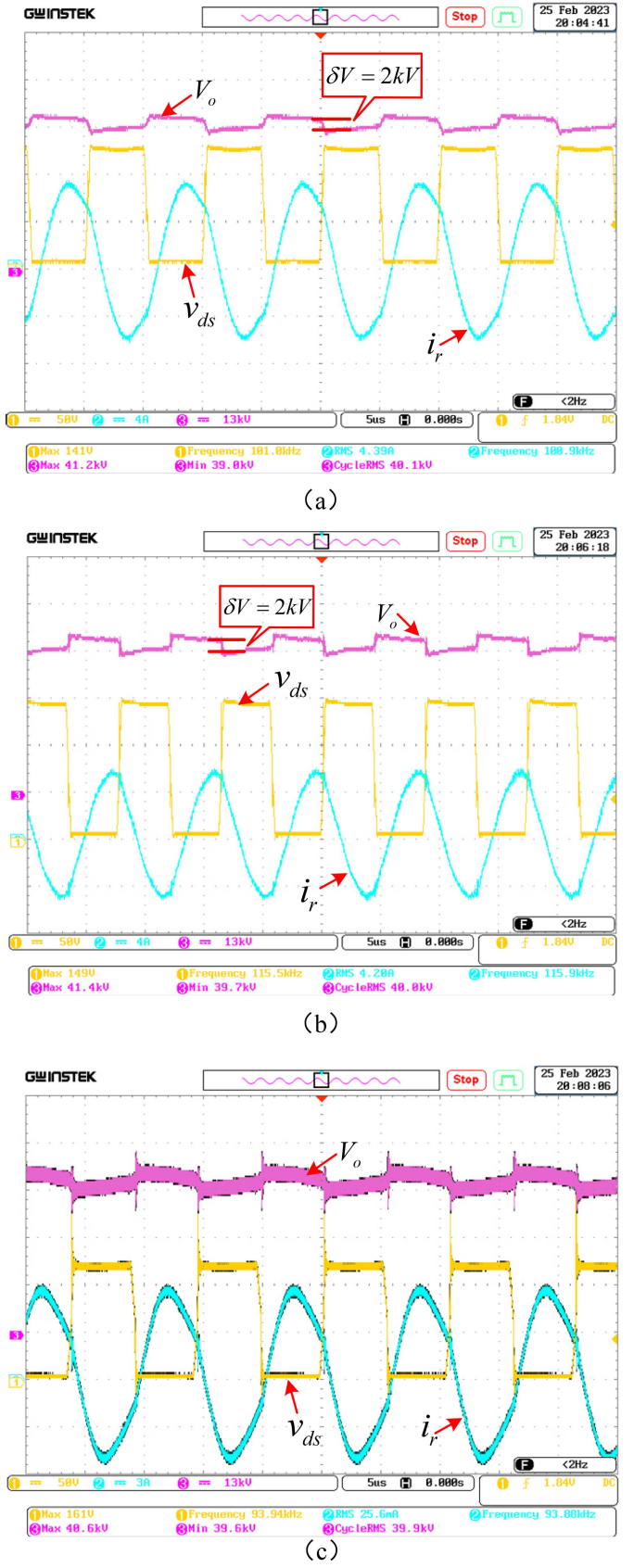


Fig. 13. Full load waveform of high voltage power supply (a) equal to f_r ; (b) greater than f_r ; (c) less than f_r .

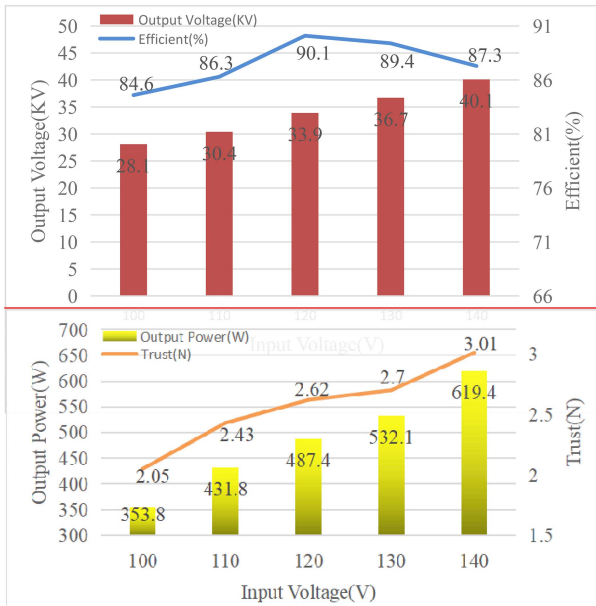


Fig. 14. Output voltage, efficiency, output power, and the thrust.



Fig. 15. Working for 3 min, the temperature of transformer.

frequency modulation control waveform is shown in Fig. 13(b). This article also tests the operation of the designed band energy below the resonant frequency, as shown in Fig. 13(c).

The efficiency under each power is tested with the input voltage as a variable. The output voltage, efficiency, output power, and thrust (generated by the electrode) are shown in Fig. 14. When the output is 33.9 kV/487.4 W, the efficiency reaches 90.1%, and the electrode generates 2.62 N thrust. When the output reaches 40.1 kV/619.4 W, the efficiency is 87.3%, and the electrode generates a 3.01 N thrust.

The temperature of the transformer after 3 min of operation (atmospheric temperature 16 °C) is shown in Fig. 15. The temperature of the transformer is 40.9 °C, which is relatively stable during the work.

The UAV using the EAD propulsion system is shown in Fig. 16. The designed HVPS is installed in the nacelle. The

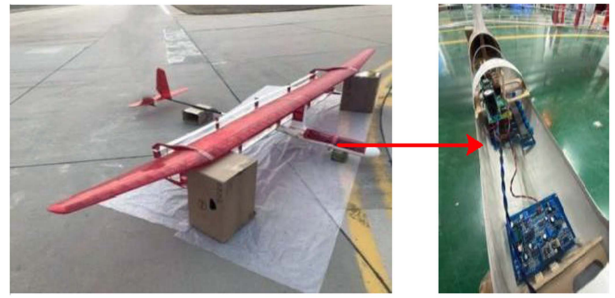


Fig. 16. UAV using EAD propulsion system.

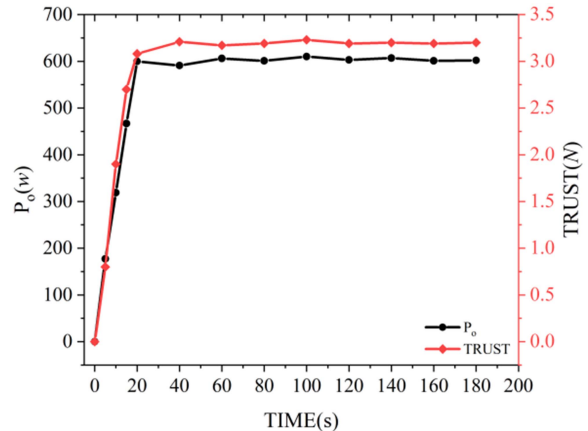


Fig. 17. Thrust test of EAD propulsion system.



Fig. 18. Continuous flight capture diagram.

HVPS generates high voltage and forms “ion wind” through the electrode installed on the wing to propel the UAV forward.

The total weight of the UAV is 2.79 kg, and the propulsion system needs to generate 3N thrust. When 35 pieces of lithium batteries are input, the HVPS can work for the 60 s under full load. The thrust test is shown in Fig. 17. To ensure the reliability of the propulsion system, the voltage source is used as the input source (Not lithium batteries), and the (3 ± 0.1) N thrust operation can be realized for 160 s. Finally, the UAV flew for the 60 s in the air with (3 ± 0.1) N full thrust, with a flight distance of 500 m. The continuous flight capture diagram is shown in Fig. 18.

VI. CONCLUSION

Aiming at the heavy weight of magnetic components in LCC HVPS, a design method of lightweight magnetic integrated transformer is proposed in this article. First, the weight-frequency relation of the high-voltage transformer is proposed. The simulation results show that there is a frequency point

$f_{\text{weight_min}}$ which minimizes the weight of the transformer core. For the high voltage transformer in a large amount of insulation material, IPOS transformer array is used, based on $f_{\text{weight_min}}$, the number of transformer selection method and insulation design method is proposed. Aiming at the magnetic integrated transformer for high voltage applications, this article proposes an asymmetric magnetic integrated transformer structure, which can adjust the position of the magnetic shunt according to the winding needs, improve the window utilization rate and reduce the weight of the magnetic core. The calculation method of magnetic integration parameters is also given. The proposed theory and method were simulated by FEA and compared with MIT's scheme. Compared with MIT's scheme, this scheme reduces 82.1 g, which is verified to be correct. Finally, the designed magnetic integrated transformer is applied to the lightweight high-voltage power supply. The experiment shows that the power output of this scheme is 40.1 kV/619.4 W with a full load, the weight of the whole machine is 423.9 g, and the power/weight ratio reaches 1.46 kW/kg. The theory and practice have a high consistency near the designed parameter points.

APPENDIX

TABLE VIII
FERRITE MAGNETIC PARAMETERS

f (kHz)	K_1 (f^j)			K_2 (f^j)		
	PC40	PC50	PC95	PC40	PC50	PC90
25	6.16 $\times 10^6$	7.13 $\times 10^6$	7.93 $\times 10^7$	2.70	2.19	3.41
50	9.16 $\times 10^6$	1.65 $\times 10^7$	1.89 $\times 10^8$	2.48	2.91	3.29
100	3.44 $\times 10^7$	3.92 $\times 10^7$	3.48 $\times 10^8$	2.63	2.85	3.21
150	7.23 $\times 10^7$	6.72 $\times 10^7$	8.93 $\times 10^8$	2.66	2.87	3.27
200	1.44 $\times 10^8$	1.30 $\times 10^8$	1.14 $\times 10^9$	2.68	2.93	3.36
250	1.49 $\times 10^8$	1.37 $\times 10^8$	1.26 $\times 10^9$	2.51	2.71	3.35
400	1.89 $\times 10^8$	2.93 $\times 10^8$	2.78 $\times 10^9$	2.28	2.69	3.34

TABLE IX
ER SERIES MAGNETIC CORE PARAMETERS

TYPE	AP (cm ⁴)	W_t (g)	P_t (W) *
ER25.5	0.3557	13.2	87
ER28/28	0.9659	26.8	240
ER28/34	1.2047	30.3	256
ER30/16	0.8546	24.6	196
ER30/35	1.3569	31.9	261
ER35/34	1.6178	43.4	286
ER35/41	2.3326	53.1	330
ER39/36	2.7713	62.7	354
ER39/42	3.4975	73.4	398
ER40/45	3.7101	78.00	421
ER42/15	4.3262	88.6	433
ER42/20	4.6661	93.4	482
ER49/54	9.0153	146.2	906

*Theoretical power of transformer operating at 101.2kHz.

The parameters in Table IX are taken into (13) to calculate the parameters under the number of different IPOS transformers.

$$\phi_{ps} = \frac{2N_P k_p I_P (R_3 + 2R_g)}{R_m [R_m + 2(R_3 + 2R_g)]} = \frac{516.07}{13.02} \times 10^{-2} = 0.396T.$$

M	2	3	4	5
AP_{\min} (cm ⁴)	2.35	1.56	1.17	0.936
Core	ER39/36	ER35/34	ER28/34	ER28/28
$(M \times W_t)g$	125.4	130.2	121.2	134

TABLE X
IPOS TRANSFORMER DESIGN PARAMETERS

$W(g)$	α	β	$F_t(\text{kHz})$	$P_o(\text{W})$	$V_o(\text{kV})$
440	0.45	4.48	101.2	600	40
η	J	$B(\text{T})$	K_u	$\sigma(\text{S/m})$	$V_{in}(\text{V})$
85%	1.09×10^6	0.372	0.382	5.7×10^7	140

TABLE XI
INTEGRATED TRANSFORMER RELUCTANCE PARAMETERS

R_{c1}	R_{c2}	R_{s1}	R_g
0.06	0.12	0.0054	7.96
R_3	R_4	R_5	R_6
0.157	0.032	0.13	0.05
R_7	R_{cc}	R_{ss}	R_m
0.08	0.03	0.003	0.4

TABLE XII
FILLING COEFFICIENT AND FREQUENCY RELATION

f (kHz)	Filling coefficient (K_u)	
	single-wire	Litz wire
25	0.4	0.3
50	0.4	0.3
100	0.394	0.3
150	0.382	0.3
200	0.374	0.3
250	0.361	0.29
400	0.344	0.24

REFERENCES

- [1] H. Xu et al., "Flight of an airplane with solid-state propulsion," *Nature*, vol. 563, no. 7732, pp. 532–535, Nov. 2018, doi: [10.1038/s41586-018-0707-9](https://doi.org/10.1038/s41586-018-0707-9).
- [2] Y. He, M. Woolston, and D. Perreault, "Design and implementation of a lightweight high-voltage power converter for electro-aerodynamic propulsion," in *Proc. IEEE 18th Workshop Control Model Power Electron.*, 2017, pp. 1–9, doi: [10.1109/COMPEL.2017.8013315](https://doi.org/10.1109/COMPEL.2017.8013315).
- [3] C. K. Gilmore and S. R. H. Barrett, "Electrohydrodynamic thrust density using positive corona-induced ionic winds for in-atmosphere propulsion," *Proc. Roy. Soc. A.*, vol. 471, no. 2175, Mar. 2015, Art. no. 20140912.
- [4] Y. He and D. J. Perreault, "Lightweight high-voltage power converters for electroaerodynamic propulsion," *IEEE J. Emerg. Sel. Topics Ind. Electron.*, vol. 2, no. 4, pp. 453–463, Oct. 2021, doi: [10.1109/JESTIE.2021.3087950](https://doi.org/10.1109/JESTIE.2021.3087950).

- [5] H. Xu, Y. He, and S. R. H. Barrett, "A dielectric barrier discharge ion source increases thrust and efficiency of electroaerodynamic propulsion," *Appl. Phys. Lett.*, vol. 114, no. 25, Jun. 2019, Art. no. 254105.
- [6] S.-H. Ahn, S.-R. Jang, and H.-J. Ryoo, "High-efficiency bidirectional three-phase LCC resonant converter with a wide load range," *IEEE Trans. Power Electron.*, vol. 34, no. 1, pp. 97–105, Jan. 2019.
- [7] S. Fan et al., "Design and analysis of high voltage power supply for industrial electrostatic precipitators," in *Proc. Int. Power Electron. Conf.*, 2018, pp. 3040–3045.
- [8] J.-S. Bae, S.-R. Jang, H.-S. Kim, C.-H. Yu, and S.-H. Ahn, "Design of ion pump power supply based on LCC resonant converter," *IEEE Trans. Plasma Sci.*, vol. 46, no. 10, pp. 3504–3511, Oct. 2018.
- [9] M. D. Antonio, S. Chakraborty, and A. Khaligh, "Planar transformer with asymmetric integrated leakage inductance using horizontal air gap," *IEEE Trans. Power Electron.*, vol. 36, no. 12, pp. 14014–14028, Dec. 2021.
- [10] Y. Wang et al., "Review of very high frequency power converters and related technologies," *Inst. Eng. Technol. Power Electron.*, vol. 13, no. 9, pp. 1711–1721, Jul. 2020.
- [11] S. Zhao, Q. Li, F. C. Lee, and B. Li, "High-frequency transformer design for modular power conversion from medium-voltage AC to 400 VDC," *IEEE Trans. Power Electron.*, vol. 33, no. 9, pp. 7545–7557, Sep. 2018.
- [12] J. Zhang, Z. Ouyang, M. C. Duffy, M. A. E. Andersen, and W. G. Hurley, "Leakage inductance calculation for planar transformers with a magnetic shunt," in *Proc. IEEE Energy Convers. Congr. Expo.*, 2013, pp. 643–648.
- [13] M. Li, Z. Ouyang, and M. A. E. Andersen, "High-frequency LLC resonant converter with magnetic shunt integrated planar transformer," *IEEE Trans. Power Electron.*, vol. 34, no. 3, pp. 2405–2415, Mar. 2019.
- [14] S. A. Ansari, J. N. Davidson, and M. P. Foster, "Fully-integrated planar transformer with a segmental shunt for LLC resonant converters," *IEEE Trans. Ind. Electron.*, vol. 69, no. 9, pp. 9145–9154, Sep. 2022.
- [15] M. Tian, J. Yin, and Y. Liu, "Magnetic integration technology in controllable reactor of transformer type constituted by various magnetic materials," *IEEE Trans. Appl. Supercond.*, vol. 24, no. 5, Oct. 2014, Art. no. 0600605.
- [16] M. X. Tian, J. N. Yin, and D. S. Yuan, "Analysis of two kinds of integrated magnetic structure of controllable reactor of transformer type," in *Proc. IEEE Int. Conf. Appl. Supercond. Electromagn. Devices*, 2013, pp. 426–429.
- [17] M. Tümay, T. Demirdelen, S. Bal, R. İ. Kayaalp, B. Doğru, and M. Aksoy, "A review of magnetically controlled shunt reactor for power quality improvement with renewable energy applications," *Renewable Sustain. Energy Rev.*, vol. 77, pp. 215–228, Sep. 2017.
- [18] J. Liu, L. Sheng, J. Shi, Z. Zhang, and X. He, "Design of high voltage, high power and high-frequency transformer in LCC resonant converter," in *Proc. 24th Annu. IEEE Appl. Power Electron. Conf. Expo.*, 2009, pp. 1034–1038.
- [19] L. Dalesandro, F. da Silveira Cavalcante, and J. W. Kolar, "Self-capacitance of high-voltage transformers," *IEEE Trans. Power Electron.*, vol. 22, no. 5, pp. 2081–2092, Sep. 2007.
- [20] N. B. Chagas and T. B. Marchesan, "Analytical calculation of static capacitance for high-frequency inductors and transformers," *IEEE Trans. Power Electron.*, vol. 34, no. 2, pp. 1672–1682, Feb. 2019.
- [21] W. Pfeiffer, "High-frequency voltage stress of insulation. methods of testing," *IEEE Trans. Elect. Insul.*, vol. 26, no. 2, pp. 239–246, Apr. 1991.
- [22] S. Mao, C. Li, W. Li, J. Popović, S. Schröder, and J. A. Ferreira, "Unified equivalent steady-state circuit model and comprehensive design of the LCC resonant converter for HV generation architectures," *IEEE Trans. Power Electron.*, vol. 33, no. 9, pp. 7531–7544, Sep. 2018.
- [23] Z. Zhao, S. He, J. Zhu, J. Lan, Y. Yang, and Y. Huang, "Design of magnetic integrated transformer for lightweight high voltage power supply to electro-aerodynamic propulsion system," in *Proc. IEEE Int. Power Electron. Appl. Conf. Expo.*, 2022, pp. 1–5.
- [24] S. Mao, Y. Chen, C. Li, W. Li, J. Popovic, and J. A. Ferreira, "A Coupled-inductor-based LCC resonant converter with the primary-Parallel–Secondary-series configuration to achieve output-voltage sharing for HV generator applications," *IEEE Trans. Power Electron.*, vol. 34, no. 7, pp. 6108–6122, Jul. 2019.
- [25] L. Deng et al., "Modeling and analysis of parasitic capacitance of secondary winding in high-frequency high-voltage transformer using finite-element method," *IEEE Trans. Appl. Supercond.*, vol. 28, no. 3, Apr. 2018, Art. no. 5500105.
- [26] D. Fu, F. C. Lee, and Y. Qiu, "A novel high-power-density three-level LCC resonant converter with constant-power-factor-control for charging applications," *IEEE Trans. Power Electron.*, vol. 23, no. 5, pp. 2411–2420, Sep. 2008.
- [27] Y. Wang, O. Lucia, Z. Zhang, Y. Guan, and D. Xu, "Review of very high frequency power converters and related technologies," *Inst. Eng. Technol. Power Electron.*, vol. 13, no. 9, pp. 1711–1721, Jul. 2020.
- [28] W.-J. Gu and R. Liu, "A study of volume and weight vs. frequency for high-frequency transformers," in *Proc. IEEE Power Electron. Specialist Conf.*, 1993, pp. 1123–1129.
- [29] N. Shafei, M. Pahlevaninezhad, H. Farzanehfard, A. Bakhtai, and P. Jain, "Analysis of a Fifth-order resonant converter for high-voltage DC power supplies," *IEEE Trans. Power Electron.*, vol. 28, no. 1, pp. 85–100, Jan. 2013.
- [30] A. Jain and I. C. Massimiani, "LCC resonant converter design and transfer function computation using FHA analysis," in *Proc. 4th Biennial Int. Conf. Nascent Technol. Eng.*, 2021, pp. 1–5.



Zhenxing Zhao was born in Hunan, China, in 1976. He received the Ph.D. degree in circuit and system from Hunan University, Changsha, China, in 2019.

He is currently an Associate Professor with Hunan Institute of Engineering, Xiangtan, China. He holds seven patents. His research interests include modeling, control and optimization of new energy and energy storage, dc microgrid and power converters.

Dr. Zhao was a recipient of four ministerial and provincial science and technology progress awards.



Jijia Zhu was born in Xiangtan, Hunan Province, in 1996. He received the bachelor's degree in electronic science and technology and master's degree in power engineering from Hunan Institute of Engineering, Xiangtan, China, in 2015 and 2022, respectively.

His current research interests include high voltage power supplies, magnetic integrated transformers, and LLC converters.



Yu-Xing Dai received the Ph.D. degree in control theory and control engineering from Central South University, Changsha, China, in 2003.

From 1995 to 2001, he was a Professor with the Department of Electronic Engineering, Hunan Normal University. From 2001 to 2011, he was a Professor and Director with the Department of Electronic Science and Technology, College of Electrical and Information Engineering, Hunan University, China. From 2011 to 2017, he was a Professor and Dean with College of Physics and Electronic Information Engineering, Wenzhou University. He is currently a Professor with the College of Electrical and Electronic Engineering, Wenzhou University and College of Electrical and Information Engineering, Hunan University, China. He is also the Director of National-Local Joint Engineering Laboratory of Digitalize Electrical Design Technology, Wenzhou University, China. He has headed more than 20 national, provincial and industrial projects. He has authored and coauthored five books, more than 100 journal and conference articles. His research interests include modeling, control and optimization of power electronic systems, microgrids and computer numerical control machine tools, computational intelligence, and engineering practice.

Dr. Dai was a recipient of 11 ministerial and provincial science and technology progress awards.



Jun Wang (Senior Member, IEEE) He received the Ph.D. degree in electrical engineering from North Carolina State University, Raleigh, NC, USA, in 2010.

He was a Device Design Engineer with Texas Instruments, Inc., Bethlehem, PA, USA, between 2010 and 2013. He was a Professor with the College of Electrical and Information Engineering, Hunan University, in 2014. He has been an Associate Editor for the IEEE JOURNAL OF EMERGING AND SELECTED TOPICS IN POWER ELECTRONICS since 2017. His research interests include power semiconductor devices and their applications in power electronics systems.



Qianming Xu (Member, IEEE) was born in Henan, China, in 1989. He received the B.S. degree in electrical engineering and automation and the Ph.D. degree in electrical engineering from Hunan University, Changsha, China, in 2012 and 2017, respectively.

Since 2017, he has been an Assistant Professor with the College of Electrical and Information Engineering, Hunan University. His research interests include modular multilevel converter, power quality control, and dc grid control.



Yachao Yang was born in Hebei, China, in 1989. He received the B.Sc. degree in electronic science and technology from Hunan Institute of Engineering, Xiangtan, China, in 2010, and the M.Sc. degree in electronics and communication engineering in 2014 from Hunan University, Changsha, China, where he is currently working toward the Ph.D. degree in electrical engineering.

His current research interests include fault analysis and protection of dc grid.



Yong Ning was born in Hunan, China, in 1980. He received the B.S. degree in electronic science and technology, M.S. degree in microelectronics and solid-state electronics, and Ph.D. degree in circuits and systems from Hunan University, Changsha, China, in 2003, 2010, and 2019, respectively.

He is currently a Postdoctoral Researcher with Hunan University. His research interests include power electronics system control and application, modeling, and control of microgrid and intelligence algorithm.



Zishun Peng (Student Member, IEEE) received the B.S. degree in electric information engineering from the Hunan Institute of Engineering, Xiangtan, China, in 2009, and the M.S. degree in computer applications technology from Wenzhou University, Wenzhou, China, in 2013. He is currently working toward the Ph.D. degree in electric engineering with the College of Electrical and Information Engineering, Hunan University, Changsha, China.

His research interests include power electronics devices and their applications.



Songming He was born in Hunan, China, in 2000. He received the bachelor's degree in automation from Hunan Institute of Engineering, Xiangtan, China, in 2023.

His current research interest includes magnetic integrated transformers.